Proceedings of the
46th IEEE Conference on Decision and Control
New Orleans, LA, USA, Dec. 12-14, 2007

Experimental evaluation of a sliding mode observer for tire-road forces and an Extended Kalman Filter for vehicle sideslip angle

Guillaume Baffet, Ali Charara, Daniel Lechner

***Abstract*— This paper proposes a new process for the estimation of tire-road forces and vehicle sideslip angle. The method strictly uses measurements from sensors potentially integrable or already integrated in recent car (yaw rate, longitudinal/lateral accelerations, steering angle and angular wheel velocities). The estimation process is based on two blocks in series: the first block contains a sliding-mode observer whose principal role is to calculate tire-road forces, while in the second block an extended Kalman filter estimates sideslip angle and cornering stiffness. More specifically, this study proposes an adaptive tire-force model that takes variations in road friction into account. The paper also presents a study of convergence for the sliding-mode observer. The estimation process was applied and compared to real experimental data, in particular wheel force measurements. Experimental results show the accuracy and potential of the estimation process.**

I. INTRODUCTION

Knowledge of lateral-dynamic variables (lateral tire forces, vehicle sideslip angle) is essential for safety enhancement, in particular for braking and trajectory-control systems. However for both technical and economical reasons some fundamental data (such as tire forces, sideslip angle) are not measurable in a standard car (even thought lateral/longitudinal accelerations, yaw rate, steering angle, wheel angular velocities may be available). As a consequence, tire forces and sideslip angle must be observed or estimated.

Vehicle-dynamic estimation has been widely discussed in the literature, e.g. [4], [5], [9], [12]. In the literature observers are often constructed by combining a single-track vehicle model with a linear tire-force model ([7], [18], [19]). This combined model, known as the linear single-track model, works well so long as the cornering stiffness (a tire-road parameter) is well known. However, when road friction changes, the real cornering stiffness varies, and so the linear single-track model is no longer satisfactory if the cornering stiffness parameter is not adapted [1].

A number of studies have described observers which take cornering stiffness variations (or road friction) into account ([14], [15]). In [14] tire-road parameters are identified with an sliding-mode observer, while in [15] tire-road forces are modeled with an integrated random walk model ($\dot{F} = \dot{F}, \ddot{F} = 0$). Some estimation processes involve the measurements of wheel torques, which nowadays have a prohibitive cost for ordinary cars. In this study, the estimation process was constructed with an eye to use only sensors potentially integrable in recent cars (accelerometer, odometer, gyrometer).

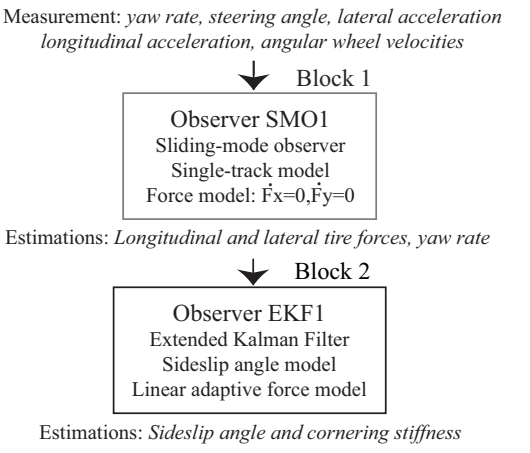

Fig. 1. Estimation process

Another particularity of this study is that the estimation process is separated into two blocks (Fig. 1). The first block estimates tire forces and yaw rate with a sliding mode observer, while the second block supplies sideslip angle and cornering stiffness estimations with an Extended Kalman Filter (EKF). In the first block, the observer (which we denote as SMO1) is constructed with a single-track model, in which forces are modeled without tire-road parameters ($\dot{F}_x = 0$, $\dot{F}_y = 0$). This formulation presents the advantage that the estimations will not be influenced by tire-road parameters. Consequently the observer may be particularly robust with respect to road friction changes. In the second block, this study proposes an observer (denoted as EKF1) developed from a sideslip angle model and a linear adaptive tire-force model. The linear adaptive force model is proposed with an eye to correcting errors resulting from road friction changes. This model adds into the linear force model a readjustment variable correcting the cornering stiffness.

The rest of the paper is organized as follows. Section 2 presents the first block modeling, analyzes the convergence properties of the sliding mode observer SMO1 and shows experimental results for the estimation of tire forces. Next, the section 3 describes the modeling of tire-road forces, proposes the observer EKF1, and presents experimental results performed within the block 2. The two observers are evaluated with respect to sideslip angle and tire force

This work was supported by the PREDIT/SARI/RADARR program.

Guillaume Baffet and Ali Charara are at the Heudiasyc Laboratory (UMR CNRS 6599), Université de Technologie de Compiègne, Centre de recherche Royallieu, BP20529 - 60205 Compiègne, France, gbaffet@hds.utc.fr, acharara@hds.utc.fr

Daniel Lechner is at the INRETS-MA Laboratory (Department of Accident Mechanism Analysis), Chemin de la Croix Blanche, 13300 Salon de Provence, France, daniel.lechner@inrets.fr

measurements. Finally, section 4 presents the conclusion.

II. TIRE-ROAD FORCE OBSERVER, SMO1

A. Modeling of the sliding mode observer SMO1

The observer SMO1 is based on the single-track model [16]. This model is represented in Fig. 2, where $\dot{\psi}$ is the yaw rate, γ_x and γ_y are the longitudinal and lateral accelerations, V_g is the vehicle velocity, β is the sideslip angle, δ is the steering angle, F_{yw1} and F_{yw2} are the front and rear lateral tire forces, F_{xw1} and F_{xw2} are the front and rear longitudinal tire forces, and F_{y1} and F_{x1} are the front lateral and longitudinal tire forces in the car body axis. L_1 and L_2 are the distances from the vehicle center of gravity to front and rear wheels, x and y are the longitudinal and lateral vehicle positions, V_{g1} and V_{g2} the front and the rear vehicle velocities, and β_1 and β_2 the front and rear sideslip angles. In order to develop an observable system (notably in the case

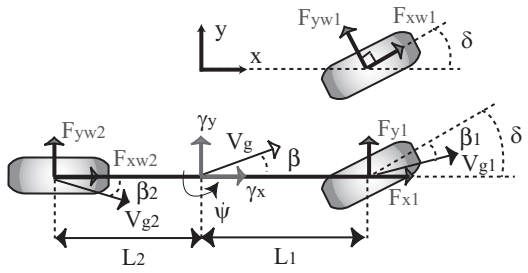

Fig. 2. Single-track model

of null steering angle), rear longitudinal tire force F_{xw2} is neglected relative to the front longitudinal force F_{x1} (assuming a front-wheel drive car, the impact of this simplification is low). The simplified equation for yaw acceleration can be formulated as the following dynamic relationship (single-track model):

$$\ddot{\psi} = \tfrac{1}{I_z}[L_1 F_{y1} - L_2 F_{yw2}], \tag{1}$$

where I_z is the yaw moment of inertia. The force evolutions are modeled as:

$$\dot{F}_{y1} = 0, \quad \dot{F}_{yw2} = 0, \quad \dot{F}_{x1} = 0. \tag{2}$$

Consider the following state $X \in R^4$ and measurement $Y \in R^3$:

$$\begin{array}{l} X = [x_1, x_2, x_3, x_4] = [\dot{\psi}, F_{y1}, F_{yw2}, F_{x1}], \\ Y = [y_1, y_2, y_3] = [\dot{\psi}, \gamma_y, \gamma_x]. \end{array} \tag{3}$$

Vectors $\widehat{X} = [\widehat{x_1}, \widehat{x_2}, \widehat{x_3}, \widehat{x_4}]$ and $\widehat{Y} = [\widehat{y_1}, \widehat{y_2}, \widehat{y_3}]$ represent the state estimations and the measurement estimations. The measurement model is:

$$\widehat{y_1} = \widehat{x_1}, \qquad \widehat{y_2} = \tfrac{\widehat{x_2} + \widehat{x_3}}{m}, \qquad \widehat{y_3} = \tfrac{\widehat{x_4}}{m}, \tag{4}$$

where m is the vehicle mass. The estimation errors for states and measurements are denoted respectively as:

$$\begin{array}{l} \widetilde{X} = [X - \widehat{X}] = [\widetilde{x_1}, \widetilde{x_2}, \widetilde{x_3}, \widetilde{x_4}], \\ \widetilde{Y} = [Y - \widehat{Y}] = [\widetilde{y_1}, \widetilde{y_2}, \widetilde{y_3}]. \end{array} \tag{5}$$

The observer SMO1 uses a sliding mode structure based principally on the works of [3] and [17]. The state estimations evolve according to the single-track model (1), the force model (2) and the sign of the measurement estimation errors:

$$\begin{array}{l} \dot{\widehat{x_1}} = \tfrac{1}{I_z}[L_1 \widehat{x_2} - L_2 \widehat{x_3}] + \Omega_1 sign(\widetilde{y_1}) \\ + \Omega_2 sign(\widetilde{y_2}) + \Omega_3 sign(\widetilde{y_3}), \\ \dot{\widehat{x_2}} = \Omega_4 sign(\widetilde{y_1}) + \Omega_5 sign(\widetilde{y_2}) + \Omega_6 sign(\widetilde{y_3}), \\ \dot{\widehat{x_3}} = \Omega_7 sign(\widetilde{y_1}) + \Omega_8 sign(\widetilde{y_2}) + \Omega_9 sign(\widetilde{y_3}), \\ \dot{\widehat{x_4}} = \Omega_{10} sign(\widetilde{y_1}) + \Omega_{11} sign(\widetilde{y_2}) + \Omega_{12} sign(\widetilde{y_3}), \end{array} \tag{6}$$

where $\Omega_1, ..., \Omega_{12}$ are the observer gains.

B. Convergence of the SMO1 observer

The aim is to set gains $\Omega_1, ..., \Omega_{12}$ which lead to the state estimation errors $\widetilde{X}$ converging toward 0. The evolution equations for the state estimation errors are the following:

$$\begin{array}{l} \dot{\widetilde{X}} = \dot{X} - \dot{\widehat{X}}, \\ \dot{\widetilde{x_1}} = \tfrac{1}{I_z}[L_1 \widetilde{x_2} - L_2 \widetilde{x_3}] - \Omega_1 sign(\widetilde{y_1}) \\ - \Omega_2 sign(\widetilde{y_2}) - \Omega_3 sign(\widetilde{y_3}), \\ \dot{\widetilde{x_2}} = -\Omega_4 sign(\widetilde{y_1}) - \Omega_5 sign(\widetilde{y_2}) - \Omega_6 sign(\widetilde{y_3}), \\ \dot{\widetilde{x_3}} = -\Omega_7 sign(\widetilde{y_1}) - \Omega_8 sign(\widetilde{y_2}) - \Omega_9 sign(\widetilde{y_3}), \\ \dot{\widetilde{x_4}} = -\Omega_{10} sign(\widetilde{y_1}) - \Omega_{11} sign(\widetilde{y_2}) \\ - \Omega_{12} sign(\widetilde{y_3}). \end{array} \tag{7}$$

Proposition (1). *Consider the following Lyapunov functions* $(\Phi_1, \Phi_2, \Phi_3, \Phi_4)$*:*

$$\begin{array}{l} \Phi_1 = \tfrac{1}{2}\widetilde{x_1}^2, \\ \Phi_2 = \tfrac{1}{2}\widetilde{x_4}^2, \\ \Phi_3 = \tfrac{1}{2}(\widetilde{x_2} + \widetilde{x_3})^2, \\ \Phi_4 = \tfrac{1}{2}(L_1 \widetilde{x_2} - L_2 \widetilde{x_3})^2. \end{array} \tag{8}$$

If the derivatives of the Lyapunov functions are negative, then the estimations $\widehat{X}$ *will converge toward the system states* X*.*

Proof (1). The Lyapunov functions $\Phi_1, ..., \Phi_4$ are positive along all state trajectories, and consequently if the derivatives $\dot{\Phi}_1, ..., \dot{\Phi}_4$ are negative, then the Lyapunov functions will converge toward zero. This entails the following convergence:

$$\begin{array}{l} \widetilde{x_1} \longrightarrow 0, \\ \widetilde{x_4} \longrightarrow 0, \\ \widetilde{x_2} + \widetilde{x_3} \longrightarrow 0, \\ L_1 \widetilde{x_2} - L_2 \widetilde{x_3} \longrightarrow 0. \end{array} \tag{9}$$

and consequently: $\widehat{x_1} \longrightarrow x_1, \widehat{x_4} \longrightarrow x_4$. Moreover the convergence $(\widetilde{x_2} + \widetilde{x_3} \longrightarrow 0)$ implies two possibilities at the switching surface: either $[\widetilde{x_2} \longrightarrow 0$ and $\widetilde{x_3} \longrightarrow 0]$, or $[\widetilde{x_2} \longrightarrow -\widetilde{x_3}]$:

- If $[\widetilde{x_2} \longrightarrow 0$ and $\widetilde{x_3} \longrightarrow 0]$, then $(\widehat{x_2} \longrightarrow x_2)$ and $(\widehat{x_3} \longrightarrow x_3)$.
- If $[\widetilde{x_2} \longrightarrow -\widetilde{x_3}]$, then the convergence $(L_1 \widetilde{x_2} - L_2 \widetilde{x_3} \longrightarrow 0)$ implies $(\widetilde{x_2}(L_1 + L_2) \longrightarrow 0)$. The parameters $(L_1 + L_2) \neq 0$, and consequently the convergence $(\widetilde{x_2} \longrightarrow 0)$, as well as $(\widetilde{x_3} \longrightarrow 0)$, are guaranteed. This entails the convergence $(\widehat{x_2}, \widehat{x_3}) \longrightarrow (x_2, x_3)$.

More specifically, gains $\Omega_1, ..., \Omega_{12}$ are chosen so as to make the Lyapunov function derivatives negative.

Proposition (2). *If the gains are set such that:*

$$\begin{array}{l} \{\Omega_1, -\Omega_7, \Omega_8, \Omega_{12}\} > 0, \\ \Omega_1 \gg \{|\Omega_2|, |\Omega_3|, |1/I_z(L_1\widetilde{x_2} - L_2\widetilde{x_3})|\}, \\ \Omega_{12} \gg \{|\Omega_{11}|, |\Omega_{10}|\}, \\ \{|\Omega_4|, |\Omega_7|, |\Omega_5|, |\Omega_8|\} \gg \{|\Omega_6|, |\Omega_9|\}, \\ \Omega_4 = -\Omega_7, \\ \Omega_5 = \Omega_8 L_2/L_1, \end{array} \quad (10)$$

then the Lyapunov function derivatives are negative and so the estimations of the yaw rate $\widehat{x_1}$, lateral tire forces $\widehat{x_2}$, $\widehat{x_3}$ and longitudinal tire force $\widehat{x_4}$ converge toward the states x_1, x_2, x_3, x_4 respectively.

Proof (2a). The derivation of the Lyapunov function Φ_1 is:

$$\begin{array}{rcl} \dot{\Phi}_1 & = & \widetilde{x_1}\dot{\widetilde{x_1}}, \\ & = & \widetilde{x_1}[\frac{1}{I_z}(L_1\widetilde{x_2} - L_2\widetilde{x_3}) - \Omega_1 sign(\widetilde{y_1}) \\ & - & \Omega_2 sign(\widetilde{y_2}) - \Omega_3 sign(\widetilde{y_3})]. \end{array} \quad (11)$$

Choosing the gains such that:

$$\begin{array}{l} \Omega_1 > 0, \\ \Omega_1 \gg \{|\Omega_2|, |\Omega_3|, |1/I_z(L_1\widetilde{x_2} - L_2\widetilde{x_3})|\}, \end{array} \quad (12)$$

the derivative becomes:

$$\dot{\Phi}_1 = -\widetilde{x_1}\Omega_1 sign(\widetilde{x_1}) < 0. \quad (13)$$

This derivative is negative, and consequently we have the convergence ($\Phi_1 \longrightarrow 0$, $\widetilde{x_1} \longrightarrow 0$), and therefore ($\widehat{x_1} \longrightarrow x_1$).

Remark (2a). At the switching surface ($\dot{\widetilde{x_1}} = 0$) this result implies:

$$sign_{eq}(\widetilde{x_1}) = \frac{1}{\Omega_1 I_z}[L_1\widetilde{x_2} - L_2\widetilde{x_3}]. \quad (14)$$

Proof (2b). The derivation of the Lyapunov function Φ_2 gives:

$$\begin{array}{rcl} \dot{\Phi}_2 & = & \widetilde{x_4}\dot{\widetilde{x_4}}, \\ \dot{\Phi}_2 & = & \widetilde{x_4}[-\Omega_{10} sign(\widetilde{y_1}) - \Omega_{11} sign(\widetilde{y_2}) \\ & - & \Omega_{12} sign(\widetilde{y_3})]. \end{array} \quad (15)$$

Using ($\Omega_{12} > 0$) and ($\Omega_{12} \gg \{|\Omega_{11}|, |\Omega_{10}|\}$), the derivative becomes negative:

$$\dot{\Phi}_2 = -(\widetilde{x_4})\Omega_{12} sign(\widetilde{x_4}) < 0, \quad (16)$$

implying the convergence ($\Phi_4 \longrightarrow 0$, $\widetilde{x_4} \longrightarrow 0$), and therefore ($\widehat{x_4} \longrightarrow x_4$).

Proof (2c). The derivative of the Lyapunov function Φ_3 is calculated as follows:

$$\begin{array}{l} \dot{\Phi}_3 = (\widetilde{x_2} + \widetilde{x_3})(\dot{\widetilde{x_2}} + \dot{\widetilde{x_3}}), \\ \dot{\Phi}_3 = (\widetilde{x_2} + \widetilde{x_3})[-(\Omega_4 + \Omega_7) sign(\widetilde{y_1}) \\ -(\Omega_5 + \Omega_8) sign(\widetilde{y_2}) - (\Omega_6 + \Omega_9) sign(\widetilde{y_3})]. \end{array} \quad (17)$$

Specifying the gains as:

$$\{|\Omega_4|, |\Omega_7|, |\Omega_5|, |\Omega_8|\} \gg \{|\Omega_6|, |\Omega_9|\}, \quad (18)$$

yields:

$$\begin{array}{rcl} \dot{\Phi}_3 & = & (\widetilde{x_2} + \widetilde{x_3})[-(\Omega_4 + \Omega_7) sign(\widetilde{y_1}) \\ & - & (\Omega_5 + \Omega_8) sign(\widetilde{x_2} + \widetilde{x_3})]. \end{array} \quad (19)$$

Moreover, if the gains are fixed such that ($\Omega_4 = -\Omega_7$) and ($\Omega_5 + \Omega_8 > 0$), this choice implies a negative $\dot{\Phi}_3$ derivative:

$$\dot{\Phi}_3 = -(\Omega_5 + \Omega_8)(\widetilde{x_2} + \widetilde{x_3}) sign(\widetilde{x_2} + \widetilde{x_3}) < 0. \quad (20)$$

Consequently this involves the convergences ($\Phi_3 \longrightarrow 0$, $\widetilde{x_2} + \widetilde{x_3} \longrightarrow 0$), and therefore ($\widehat{x_2}, \widehat{x_3}$) $\longrightarrow (x_2, x_3)$ (proposition 1).

Proof (2d). The derivative calculation of Lyapunov function Φ_4 gives:

$$\begin{array}{l} \dot{\Phi}_4 = (L_1\widetilde{x_2} - L_2\widetilde{x_3})(L_1\dot{\widetilde{x_2}} - L_2\dot{\widetilde{x_3}}), \\ \dot{\Phi}_4 = (L_1\widetilde{x_2} - L_2\widetilde{x_3})[(-L_1\Omega_4 + L_2\Omega_7) sign(\widetilde{y_1}) \\ +(-L_1\Omega_5 + L_2\Omega_8) sign(\widetilde{y_2})]. \end{array} \quad (21)$$

Applying the result (14) and choosing ($\Omega_4 = -\Omega_7$), equation (21) becomes:

$$\begin{array}{rcl} \dot{\Phi}_4 & = & (L_1\widetilde{x_2} - L_2\widetilde{x_3})[\frac{\Omega_7}{\Omega_1 I_z}(L_1 + L_2)(L_1\widetilde{x_2} \\ & - & L_2\widetilde{x_3}) + (-L_1\Omega_5 + L_2\Omega_8) sign(\widetilde{y_2})]. \end{array} \quad (22)$$

Specifying ($\Omega_5 = \Omega_8 L_2/L_1$) and ($\Omega_7 < 0$) means that the derivative:

$$\dot{\Phi}_4 = \frac{\Omega_7(L_1+L_2)}{\Omega_1 I_z}(L_1\widetilde{x_2} - L_2\widetilde{x_3})^2 < 0, \quad (23)$$

becomes negative, which implies the convergences ($\Phi_4 \longrightarrow 0$), and therefore ($L_1\widetilde{x_2} - L_2\widetilde{x_3} \longrightarrow 0$). Consequently this induces the convergence ($\widehat{x_2}, \widehat{x_3}$) $\longrightarrow (x_2, x_3)$ (proposition 1).

C. Experimental results - observer SMO1

The INRETS MA vehicle (see figure 3) is a Peugeot 307

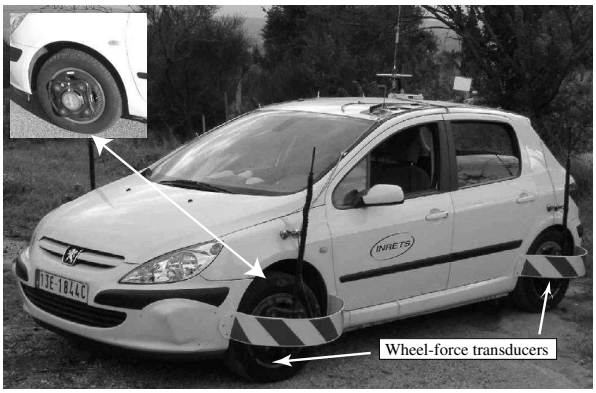

Fig. 3. INRETS MA Laboratory's experimental vehicle

equipped with a number of sensors including centimetric GPS, accelerometers, gyrometers, steering angle, Correvit and dynamometric hubs. The Correvit is fixed a the rear of the vehicle so this sensor gives validation measurements of the rear sideslip angle and the rear vehicle velocity. The dynamometric hubs are placed at the four wheels and provide validation measurements of tire-forces.

This study included an experimental test representative of

both longitudinal and lateral dynamic behaviors. The vehicle trajectory and the acceleration diagram are shown in Fig.4. During the test, the vehicle first accelerated up to $\gamma_x = 0.3$ g (situation 1), then negotiated a slalom ($-0.6\ g < \gamma_y < 0.6$ g) (situation 2), before finally decelerating to $\gamma_x \approx -0.5$ g (situation 3). The estimations of the tire forces along the

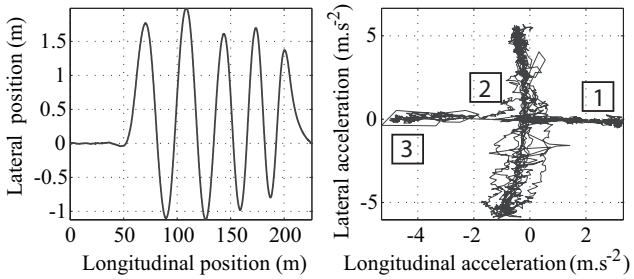

Fig. 4. Slalom experimental test, vehicle positions, acceleration diagram

wheel axis are obtained by applying the following equations:

$$\begin{aligned} F_{xw1} &= F_{x1}\cos(\delta) + F_{y1}\sin(\delta), \\ F_{yw1} &= F_{y1}\cos(\delta) - F_{x1}\sin(\delta). \end{aligned} \tag{24}$$

The estimation results are presented on two ways: figures of estimation results compared with measurements, and tables of normalized errors. The normalized error ε_z for an estimation z is defined as [18]:

$$\varepsilon_z = \frac{100\|z - z_{measurement}\|}{\max\|z_{measurement}\|}. \tag{25}$$

Figs. 5 and tables I present SMO1 observer results. The state estimations were initialized with the maximum measurements during the test (for instance $\widehat{x_{2(t=0)}} = 5448N$ in the slalom test). In spite of these false initializations the estimations converge quickly to the measurements, showing the good convergence properties of the observer. Moreover, SMO1 observer produces satisfactory estimations close to measurements (normalized mean errors and standard deviation less than 5 % in table I). These good experimental results confirm that the observer approach may be appropriate for the estimation of tire-forces.

III. SIDESLIP ANGLE AND WHEEL CORNERING STIFFNESS OBSERVER, EKF1

This section introduces tire-force modeling and presents the observer EKF1 for the estimation of sideslip angle and wheel cornering stiffness.

TABLE I

EXPERIMENTAL RESULTS, SMO1 OBSERVER, MAXIMUM ABSOLUTE VALUES, NORMALIZED MEAN ERRORS AND STANDARD DEVIATION (STD)

Slalom	max $\|\quad\|$	Mean	Std
F_{y1}	6282 N	4.1%	3.8%
F_{y2}	3663 N	2.2%	1.9%
F_{x1}	6181 N	3.8%	3.6%
$\dot{\psi}$	33.6 $^o/s$	0.5%	0.3%

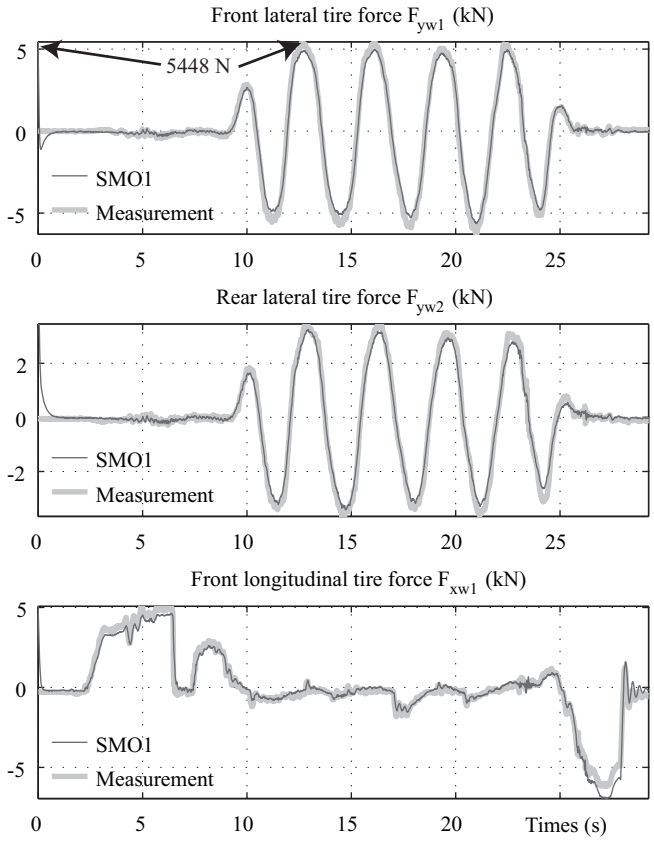

Fig. 5. Experimental test (Slalom). Sliding mode observer SMO1 results in comparison with experimental measurements

A. Modeling of the extended Kalman filter EKF1

The filter EKF1 is constructed by combining models characterizing the vehicle sideslip angle and the tire-road contact forces. The sideslip angle evolution is formulated by using the single-track model [16]:

$$\begin{aligned} \dot{\beta} = \tfrac{1}{mV_g}[&F_{xw1}\sin(\delta-\beta) + F_{yw1}\cos(\delta-\beta) \\ &+F_{yw2}\cos(\beta)] - \dot{\psi}. \end{aligned} \tag{26}$$

The wheel sideslip angles and the center of gravity sideslip angle are linked with the following relationships:

$$\beta_1 = \delta - \beta - \tfrac{L_1\dot{\psi}}{V_g}, \quad \beta_2 = -\beta + \tfrac{L_2\dot{\psi}}{V_g}. \tag{27}$$

The tire forces are usually modeled as a function of the slips between tire and road ([2], [13]), such as the wheel longitudinal slip and the wheel sideslip angle. Fig. 6 illustrates different lateral tire-force models (linear, linear adaptive and Burckhardt for various road surfaces, [7]). For normal driving situations, lateral tire forces are usually considered linear with respect to sideslip angle (linear model, cumulative lateral tire-force for each axle):

$$F_{ywi}(\beta_i) = 2C_i\beta_i, \qquad i = 1, 2, \tag{28}$$

where C_i is the wheel cornering stiffness (a parameter closely related to tire-road friction).

When road friction changes or when the nonlinear tire

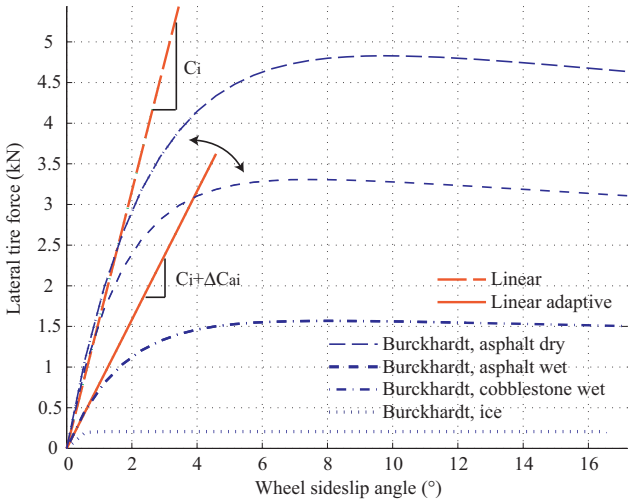

Fig. 6. Lateral tire force models: linear, linear adaptive, Burckhardt for various road surfaces

domain is reached, "real" cornering stiffness varies. In order to take this variation into account a linear adaptive tire-force model is proposed. This model is based on the linear model to which a readjustment variable ΔC_{ai} has been added to correct wheel cornering stiffness errors:

$$F_{ywi}(\beta_i) = 2(C_i + \Delta C_{ai})\beta_i. \tag{29}$$

The variable ΔC_{ai} is included in the state vector of the EKF1 observer and its evolution equation is formulated according to the model ($\Delta \dot{C}_{ai} = 0$).
State $X' \in R^3$, input $U' \in R^4$ and measurement $Y' \in R^3$ are chosen as:

$$\begin{aligned} X' &= [x'_1, x'_2, x'_3] = [\beta, \Delta C_{a1}, \Delta C_{a2}], \\ U' &= [u'_1, u'_2, u'_3, u'_4] = [\delta, \dot{\psi}, V_g, F_{xw1}], \\ Y' &= [y'_1, y'_2, y'_3] = [F_{yw1}, F_{yw2}, \gamma_y]. \end{aligned} \tag{30}$$

The measurement model is

$$\begin{aligned} y'_1 &= 2(C_1 + x'_2)\beta_1, \\ y'_2 &= 2(C_2 + x'_3)\beta_2, \\ y'_3 &= \tfrac{1}{m}[2(C_1 + x'_2)\beta_1 \cos(u'_1) + 2(C_2 + x'_3)\beta_2 \\ &+ u'_4 \sin(u'_1)]. \end{aligned} \tag{31}$$

Consider the state estimation denoted as $\widehat{X}' = [\widehat{x_1}', \widehat{x_2}', \widehat{x_3}']$. The state evolution model of EKF1 is:

$$\begin{aligned} \dot{\widehat{x_1}}' &= \tfrac{1}{mu'_3}[u'_4 \sin(u'_1 - \widehat{x_1}') + F_{auxi1} \cos(u'_1 - \widehat{x_1}') \\ &+ F_{auxi2} \cos(\widehat{x_1}')] - u'_2, \\ \dot{\widehat{x_2}}' &= 0, \\ \dot{\widehat{x_3}}' &= 0, \end{aligned} \tag{32}$$

where the auxiliary variables F_{auxi1} and F_{auxi2} are calculated as:

$$\begin{aligned} F_{auxi1} &= 2(C_1 + \widehat{x_2}')(u'_1 - \widehat{x_1}' - \tfrac{L_1 u'_2}{u'_3}), \\ F_{auxi2} &= 2(C_2 + \widehat{x_3}')(-\widehat{x_1}' + \tfrac{L_2 u'_2}{u'_3}). \end{aligned} \tag{33}$$

The extended Kalman filter EKF1 is based on a study by [6] and constructed according to an algorithm proposed in [10]. An observability function was calculated using a Lie derivative method [11]. Rank of the observability function, which were calculated along experimental trajectories, corresponded to the state vector dimension (3), consequently system EKF1 was locally observable.

B. Experimental results - observer EKF1

In order to demonstrate the improvement provided by the observer using the linear adaptive force model (29), another observer constructed with a linear force model (28) was used in comparison (denoted Orl, described in [1]). The robustnesses of the two observers was tested with respect to tire-road friction variations by performing the tests with different cornering stiffness parameters ($[C_1, C_2] * 0.5, 1, 1.5$ with $C_1 = 65000\ N.rad^{-1}$ and $C_2 = 50000\ N.rad^{-1}$).
Fig. 7 and Table II show the estimations results of Orl observer (using the linear force model) for the rear sideslip angle. The Orl observer gives good results when cornering stiffnesses are approximately known ($[C_1, C_2] * 1$). However, this observer is not robust when cornering stiffnesses change ($[C_1, C_2] * 0.5, 1.5$).
Fig. 8(A) and Table II present the rear sideslip estimation obtained with the observer EKF1 (using the linear adaptive tire-force model). The performance robustness of EKF1 is very good since rear sideslip angle is well estimated irrespective of cornering stiffness settings. This result is confirmed by the EKF1 normalized errors (Table II) which are approximately similar (around 5 %).

TABLE II
EXPERIMENTAL TEST, ORL AND EKF1 OBSERVERS, MAXIMUM ABSOLUTE VALUES AND NORMALIZED MEAN ERRORS OF THE REAR SIDESLIP ANGLE

Slalom	$(C_1, C_2) * 0.5$	(C_1, C_2)	$(C_1, C_2) * 1.5$
$\max \|\beta_2\|$	5.7^o	5.7^o	5.7^o
Orl	13.1%	5.7%	7.8%
SMO1	5.3%	5.0%	5.1%

Figs. 8(B,C) present the front and rear cornering stiffness estimations ($C_i + \Delta C_i$). It can be seen that the cornering stiffness estimations remain approximately constant when the lateral dynamic (sideslip angles, lateral tire forces) is low,

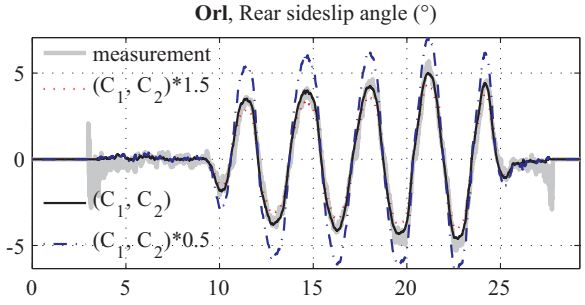

Fig. 7. Experimental test, Observer Orl, with different cornering stiffness settings $[(C_1, C_2) = (65000, 50000) * (0.5, 1, 1.5)\ N.rad^{-1}]$. Rear sideslip angle estimations.

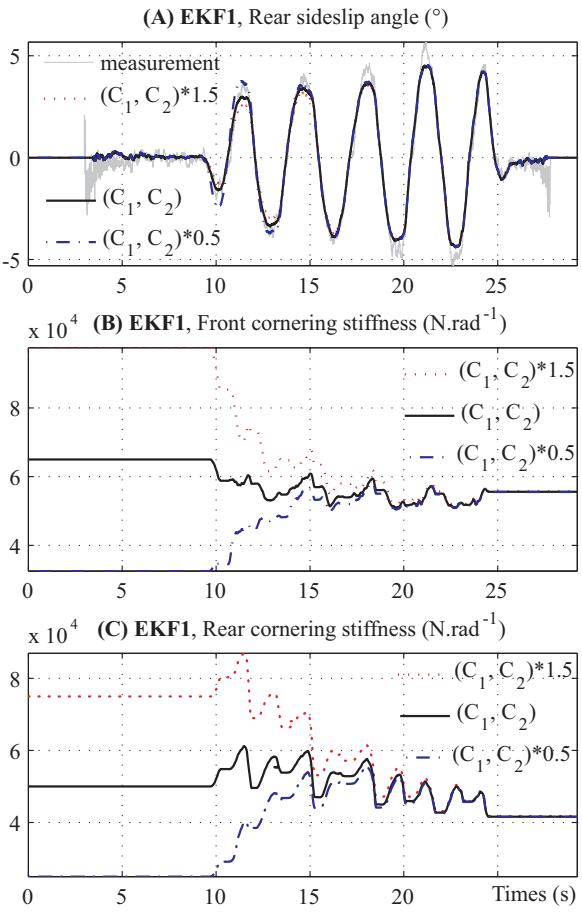

Fig. 8. Experimental test, Observer EKF1, with different cornering stiffness settings $[(C_1, C_2) = (65000, 50000) * (0.5, 1, 1.5)\ N.rad^{-1}]$. **(A) EKF1**, rear sideslip angle estimations. **(B) EKF1**, front cornering stiffness estimations $C_1 + \Delta C_{a1}$. **(C) EKF1**, rear cornering stiffness estimations $C_2 + \Delta C_{a2}$. At the beginning of the test, the variables ΔC_{a1} and ΔC_{a2} were initialized with zero.

that is to say during the first 9 s of the test. Then, at the beginning of the slalom at 10 s the lateral dynamic becomes sufficiently large, and the estimations converge quickly to the same values.

IV. CONCLUSIONS AND FUTURE WORKS

This study deals with two vehicle-dynamic observers constructed for use in a two-block estimation process. The first observer (block 1) mainly estimates tire-forces (without explicit tire-force model), while the second observer (block 2) calculates sideslip angle (with adaptation of the cornering stiffnesses).

The first observer SMO1, a sliding mode observer, was constructed by finding the gains with respect to the convergence. The experimental evaluations of SMO1 are satisfactory, showing excellent estimations close to the measurements and good convergence properties. The second observer EKF1, an extended Kalman filter, was developed with an adaptive tire-force model. This observer was tested for different cornering stiffness settings and was compared with another observer using a linear tire-force model (Orl). Results shows that the observer Orl is not robust when cornering stiffness parameters change, whereas the observer EKF1 (using the linear adaptive force model) gives good estimations of the sideslip angle. This result justifies the use of an adaptive tire-force model to take into account road friction changes.

Future studies will improve vehicle-road models. Subsequent vehicle-road models will take into account roll, vertical dynamics and tire elasto-kinematics. Moreover, experimental tests will be done, notably on different road surfaces.

REFERENCES

[1] G. Baffet, J. Stephant and A. Charara, "Sideslip angle, Lateral tire force and road friction estimation in simulations and experiments", *Proceedings of the IEEE Conference on Control Application, CCA, Munich, Germany*, 2006b, pp 903–908.

[2] Canudas-De-Wit, C., Tsiotras, P., Velenis, E., M. Basset and G. Gissinger, "Dynamic friction models for road/tire longitudinal interaction", *Vehicle System Dynamics*, 2003, vol. 39, pp 189-226.

[3] S. Drakunov and V. Utkin, "Sliding mode observers", *IEEE Conference on Decision and Control*, 1995, pp 3376-3379.

[4] F. Gustafsson, "Slip-based Tire-Road Friction Estimation", *Automatica*, 1997, vol. 33, no 6, pp. 1087-1099.

[5] Y.H.J. Hsu and J.C. Gerdes, "A feel for the road: a method to estimate tire parameters using steering torque", *Proceedings of the 8th International Symposium on Advanced Vehicle Control, AVEC, Taipei, Taiwan*, 2006, 835–840.

[6] R.E. Kalman, "A New Approach to Linear Filtering and Prediction Problems", *Transactions of the ASME - Journal of Basic Engineering*, 1960, vol. 82, série D, pp. 35-45.

[7] U. Kiencke and L. Nielsen, Automotive control system, *Springer*, 2000.

[8] M. Lakehal-ayat, H.E. Tseng, Y. Mao and j. Karidas, "Disturbance Observer for Lateral Velocity Estimation", *Proceedings of the 8th International Symposium on Advanced Vehicle Control AVEC, Taipei, Taiwan*, 2006, 889–894.

[9] D. Lechner, "Analyse du comportement dynamique des vehicules routiers legers: developpement d'une methodologie appliquee a la securite primaire", *Ph.D. dissertation, Ecole Centrale de Lyon*, 2002, Lyon, France.

[10] S.G. Mohinder and P.A. Angus, Kalman filtering theory and practice. *Prentice hall*, 1993.

[11] H. Nijmeijer and A.J. Van der Schaft, Nonlinear Dynamical Control Systems, *Springer-Verlag*, 1990.

[12] E. Ono, K. Asano, M. Sugai, S. Ito, M. Yamamoto, M. Sawada and Y. Yasui, "Estimation of automotive tire force characteristics using wheel velocity", *Control Engineering Practice*, 2003, Vol. 11, Issue 12, pp. 1361-137.

[13] H.B. Pacejka and E. Bakker, "The magic formula tyre model", *Proceedings of* 1^{st} *Int. colloq. on tyre models for vehicle dynamics analysis*, 1991, pp. 1-18.

[14] A. Rabhi, N.K. M'Sirdi, N. Zbiri and Y. Delanne, "Vehicle-road interaction modelling for estimation of contact forces", *Vehicle System Dynamics*, Taylor and Francis, 2005, Vol. 43, Supplement, pp. 403-411.

[15] L. Ray, "Nonlinear Tire Force Estimation and Road Friction Identification: Simulation and Experiments", *Automatica*, 1997, vol. 33, no. 10, pp 1819-1833.

[16] M.L. Segel, "Theorical prediction and experimental substantiation of the response of the automobile to steering control", *Proceedings of automobile division of the institut of mechanical engineers*, 1956, vol. 7, pp 310-330.

[17] J. Slotine, J. Hedrick and E. Misawa, "On sliding observer for nonlinear systems", *Journal of mathematical systems. Estimation and control*, 1987, vol. 109, pp 245-259.

[18] J. Stephant, A. Charara and D. Meizel, "Virtual sensor, application to vehicle sideslip angle and transversal forces", *IEEE Transactions on Industrial Electronics*, 2004, 51, 278-289.

[19] A.Y. Ungoren, H. Peng and H.E. Tseng, "A study on lateral speed estimation methods", *Int. J. Vehicle Autonomous Systems*, 2004, vol. 2, Nos. 1/2, pp. 126-144.